

Non-Gaussian Fingerprints of Self-Interacting Curvaton

Kari Enqvist^{a,b,*}, Sami Nurmi^{c,†}, Olli Taanila^{a,b,‡}, Tomo Takahashi^{d,§}

^a*Physics Department, FIN-00014 University of Helsinki, Finland;*

^b*Helsinki Institute of Physics, FIN-00014 University of Helsinki, Finland;*

^c*Institute for Theoretical Physics, University of Heidelberg, 69120 Heidelberg, Germany;*

^d*Department of Physics, Saga University, Saga 840-8502, Japan*

ABSTRACT: We investigate non-Gaussianities in self-interacting curvaton models treating both renormalizable and non-renormalizable polynomial interactions. We scan the parameter space systematically and compute numerically the non-linearity parameters f_{NL} and g_{NL} . We find that even in the interaction dominated regime there are large regions consistent with current observable bounds. Whenever the interactions dominate, we discover significant deviations from the relations $f_{\text{NL}} \sim r_{\text{dec}}^{-1}$ and $g_{\text{NL}} \sim r_{\text{dec}}^{-1}$ valid for quadratic curvaton potentials, where r_{dec} measures the curvaton contribution to the total energy density at the time of its decay. Even if $r_{\text{dec}} \ll 1$, there always exists regions with $f_{\text{NL}} \sim 0$ since the sign of f_{NL} oscillates as a function of the parameters. While g_{NL} can also change sign, typically g_{NL} is non-zero in the low- f_{NL} regions. Hence, for some parameters the non-Gaussian statistics is dominated by g_{NL} rather than by f_{NL} . Due to self-interactions, both the relative signs of f_{NL} and g_{NL} and the functional relation between them is typically modified from the quadratic case, offering a possible experimental test of the curvaton interactions.

KEYWORDS: Curvaton, non-Gaussianities, self-interactions.

*E-mail: kari.enqvist@helsinki.fi

†E-mail: s.nurmi@thphys.uni-heidelberg.de

‡E-mail: olli.taanila@iki.fi

§E-mail: tomot@cc.saga-u.ac.jp

Contents

1. Introduction	1
2. Non-Gaussianities in self-interacting curvaton models	2
2.1 Analytical considerations	4
3. Renormalizable potential	5
4. Non-renormalizable potentials	7
4.1 Qualitative features and differences from naïve expectations	7
4.2 Allowed regions of parameter space	10
5. Discussion	13

1. Introduction

In the curvaton scenario [1], primordial perturbations originate from quantum fluctuations of a curvaton field σ which remains effectively massless during inflation and contributes very little to the total energy density. After the end of inflation, the curvaton energy density stays nearly constant until the field becomes effectively massive, while the dominating radiation component generated at reheating scales as $\rho_{\text{rad}} \propto a^{-4}$. The curvaton contribution to the total energy density therefore grows rapidly after the end of inflation and its perturbations start to affect the expansion history. In this way the initial isocurvature fluctuations of the curvaton field get gradually converted into adiabatic curvature perturbations. The observed primordial perturbation can originate solely from the curvaton perturbations, although scenarios with mixed inflaton and curvaton perturbations are also possible [2]. As the curvaton finally decays and the decay products thermalize, the adiabatic hot big bang epoch is recovered and the curvature perturbation freezes to a constant value on superhorizon scales.

Predictions of the curvaton scenario depend crucially on the form of the curvaton potential [3, 4, 5, 6, 7, 8, 9, 10, 11] (and the background evolution [12]). Although the curvaton must be weakly coupled to the thermal bath after the end of inflation, interactions of some type should be present in realistic models.

In the present paper, we consider self-interacting curvaton models with the generic potential

$$V = \frac{1}{2}m^2\sigma^2 + \lambda\sigma^{n+4}, \quad (1.1)$$

with $n = 0, 2, 4, 6$ and $\lambda > 0$. We set $M_{\text{P}} = (8\pi G)^{-1/2} \equiv 1$ throughout the paper. In [10] it was found numerically that the predictions of such models can deviate significantly from the extensively studied quadratic case [13], as shown already in [4, 5] in the limit of small interactions. For non-quadratic potentials the amplification of curvaton energy after inflation is less efficient than in the quadratic case, but one may still generate the observed amplitude of primordial perturbation since the curvaton perturbation generated during inflation, $\delta\sigma_*/\sigma_*$, can be larger than 10^{-5} . As shown in [10], the correct amplitude can be achieved in a relatively large part of the parameter space.

However, the dynamics is very complicated and, for non-renormalizable potentials, the curvature perturbation $\zeta = \Delta N$ (here understood to contain all orders of perturbation theory) displays oscillations as a function of the initial curvaton field value σ_* . This reflects the dynamics of transition from curvaton oscillations in the non-quadratic part of the potential to the quadratic part, as discussed in [10]. For the (marginally) renormalizable case, $n = 0$, the transition does not give rise to an oscillatory behaviour of ζ but nevertheless affects the final value of the perturbation.

Here we extend the analysis of [10] and focus on primordial non-Gaussianities generated in the class of curvaton models with the potential (1.1). We use the ΔN formalism and solve the equations of motion numerically. We perform a systematic scan through the parameter space and evaluate the non-linearity parameters f_{NL} and g_{NL} . Combining this information with the amplitude of perturbations, we find the regions of the parameter space that are consistent with current observational constraints. As a result of the oscillatory behaviour of $\zeta(\sigma_*)$, the observational constraints on the self-interacting model (1.1) differ significantly from the quadratic case.

The paper is organized as follows. In Sect. 2 we give our basic definitions and discuss the generic features of the non-linearity parameters f_{NL} and g_{NL} . In Sect. 3, we tackle the special case of the renormalizable, four point interaction, for which we can use the analytical estimates derived in [10]. In Sect. 4, we extend our analysis to non-renormalizable interactions with $n = 2, 4, 6$ by resorting to numerics. This section contains our main results. Finally, in Sect. 5 we present our conclusions.

2. Non-Gaussianities in self-interacting curvaton models

We use the δN formalism [14, 15] and assume that the curvature perturbation arises solely from perturbations of a single curvaton field generated during inflation. The

curvature perturbation ζ can then be expanded as

$$\zeta(t, \mathbf{x}) = N'(t, t_*)\delta\sigma_*(\mathbf{x}) + \frac{1}{2}N''(t, t_*)\delta\sigma_*(\mathbf{x})^2 + \frac{1}{6}N'''(t, t_*)\delta\sigma_*(\mathbf{x})^3 \dots \quad (2.1)$$

Here $N(t, t_*)$ is the number of e-foldings from an initial spatially flat hypersurface with fixed scale factor $a(t_*)$ to a final hypersurface with fixed energy density $\rho(t)$, evaluated using the FRW background equations. The final time t should be chosen as some (arbitrary) time event after the curvaton decay. The prime denotes a derivative with respect to the initial curvaton value σ_* . Here we take t_* to be some time during inflation soon after all the cosmologically relevant modes have exited the horizon and assume the curvaton perturbations $\delta\sigma_*$ are Gaussian at this point. The expansion (2.1) is then of the form

$$\zeta(t, \mathbf{x}) = \zeta_g(t, \mathbf{x}) + \frac{3}{5}f_{\text{NL}}\zeta_g(t, \mathbf{x})^2 + \frac{9}{25}g_{\text{NL}}\zeta_g(t, \mathbf{x})^3 + \dots \quad (2.2)$$

where $\zeta_g(t, \mathbf{x})$ is a Gaussian field and the non-linearity parameters are given by

$$f_{\text{NL}} = \frac{5}{6} \frac{N''}{N'^2} \quad (2.3)$$

$$g_{\text{NL}} = \frac{25}{54} \frac{N'''}{N'^3} \quad (2.4)$$

Here we neglect all the scale dependence of the non-linearity parameters [16]. With this assumption and neglecting higher order perturbative corrections, the constants f_{NL} and g_{NL} measure the amplitudes of the three- and four-point correlators of ζ respectively.

We assume the curvaton obeys slow roll dynamics during inflation and introduce a parameter r_* to measure its contribution to the total energy density ρ at t_*

$$r_* = \left. \frac{\rho_\sigma}{\rho} \right|_{t_*} \simeq \frac{V(\sigma_*)}{3H_*^2} \ll 1 \quad (2.5)$$

The inflationary scale H_* appears as a free parameter in our analysis, up to certain model dependent consistency conditions. Assuming inflation is driven by a slowly rolling inflaton field, we need to require $H_* \ll 10^{-5}\sqrt{\epsilon}$ in order to make the inflaton contribution to ζ negligible. In this setup we also need to adjust $\epsilon = -\dot{H}_*/H_*^2$, determined by the inflaton dynamics, to give the correct spectral index, $n - 1 = 2\epsilon - 2\eta_{\sigma\sigma}$ [17]. The curvaton contribution, $\eta_{\sigma\sigma} = V''(\sigma_*)/3H_*^2$, is typically negligible because of the subdominance of the curvaton. The curvaton mass needs to be small but the same also holds for the inflaton mass. We assume this minimal setup in the current work for definiteness since our main goal is to discuss the new features arising from curvaton self-interactions.

After the end of inflation, we assume the inflaton decays completely into radiation and the universe becomes radiation dominated. We introduce a phenomenological

decay constant Γ to account for the coupling between the radiation and the curvaton component. The evolution of the coupled system is given by

$$\ddot{\sigma} + (3H + \Gamma)\dot{\sigma} + m^2\sigma + \lambda(n + 4)\sigma^{n+3} = 0 \quad (2.6)$$

$$\dot{\rho}_r = -4H\rho_r + \Gamma\dot{\sigma}^2 \quad (2.7)$$

$$3H^2 = \rho_r + \rho_\sigma . \quad (2.8)$$

The initial conditions are given by $\rho_r = 3H_*^2$ and $\rho_\sigma = V(\sigma_*) = r_*/(1 - r_*)\rho_r$ specified at time t_* corresponding to the end of inflation. We also put $\dot{\sigma} = 0$. Given the parameters n , λ and m , which determine the potential (1.1), and the two initial conditions r_* and H_* , we can calculate N in (2.1) from this set of equations. To find the curvature perturbation, we set $\delta\sigma_* = H_*/(2\pi)$ and compute $\zeta = N(\sigma_* + \delta\sigma_*) - N(\sigma_*)$. For a given set of parameters, we adjust the decay width Γ so that the observed amplitude is obtained, $\zeta \sim 10^{-5}$ [18].

We treat Γ as a free parameter since we have not specified the curvaton couplings to other matter, in particular to the Standard Model fields. However, since the primordial perturbations have been observed to be adiabatic to a high degree [18], the curvaton should decay before dark matter decouples in order not to produce isocurvature modes. Assuming the freeze-out temperature for an LSP type dark matter model with $T_{\text{DM}} \sim \mathcal{O}(10)$ GeV, this translates to a rough bound

$$\Gamma \gtrsim 10^{-15} \text{GeV} = 10^{-33} . \quad (2.9)$$

While this bound could be relaxed in non-minimal constructions, we assume it for definiteness for the rest of our work.

2.1 Analytical considerations

In Sect. 4 we solve the set of equations (2.6) - (2.8) numerically and compute the resulting curvature perturbation (2.1) and the non-linearity parameters (2.3) and (2.4). However to gain some physical insight of the results, it is useful to start by discussing generic approximative analytic expressions that can be derived for f_{NL} and g_{NL} . Assuming the curvaton decays instantaneously [19] at $H_{\text{dec}} = \Gamma$ and neglecting the coupling between curvaton and radiation before t_{dec} , one can estimate the non-linearity parameters by [5, 20, 21]

$$f_{\text{NL}} = \frac{5}{3r_{\text{dec}}} \left(1 + \frac{\sigma_{\text{osc}}\sigma''_{\text{osc}}}{(\sigma'_{\text{osc}})^2} \right) - \frac{5}{3} - \frac{5r_{\text{dec}}}{8} \quad (2.10)$$

$$g_{\text{NL}} = \frac{25}{54} \left[\frac{4}{r_{\text{dec}}^2} \left(\frac{\sigma_{\text{osc}}^2\sigma'''_{\text{osc}}}{(\sigma'_{\text{osc}})^3} + \frac{3\sigma_{\text{osc}}\sigma''_{\text{osc}}}{(\sigma'_{\text{osc}})^2} \right) - \frac{12}{r_{\text{dec}}} \left(1 + \frac{\sigma_{\text{osc}}\sigma''_{\text{osc}}}{(\sigma'_{\text{osc}})^2} \right) + \frac{1}{2} \left(1 + \frac{\sigma_{\text{osc}}\sigma''_{\text{osc}}}{(\sigma'_{\text{osc}})^2} \right) + \frac{30r_{\text{dec}}}{4} + \frac{27r_{\text{dec}}^2}{16} \right] . \quad (2.11)$$

Here $r_{\text{dec}} = \rho_\sigma/\rho|_{\text{dec}} \sim \sigma_{\text{osc}}^2(m/\Gamma)^{1/2}$ and σ_{osc} is the envelope of the oscillating curvaton field at some time t_{osc} after the beginning of oscillations in the quadratic part of the potential. The results are independent of the precise choice of t_{osc} .

If the curvaton potential is exactly quadratic, $\sigma_{\text{osc}} \propto \sigma_*$ and the non-linearity parameters f_{NL} and g_{NL} are uniquely determined by r_{dec} , i.e. by the curvaton energy density at the time of decay. However, interactions in general make the function $\sigma_{\text{osc}}(\sigma_*)$ non-linear and, especially in the limit $r_{\text{dec}} \ll 1$, the quadratic predictions can be greatly altered due to the derivative terms in (2.10) and (2.11). If the interactions dominate the curvaton dynamics at the time of inflation, the non-linearity parameters can only very crudely be approximated by $f_{\text{NL}} \sim r_{\text{dec}}^{-1}$ and $g_{\text{NL}} \sim r_{\text{dec}}^{-2}$. As will be discussed in Sect. 4, in the interacting case the non-linearity parameters can deviate significantly from these naïve estimates. This follows from the non-trivial behaviour of derivatives of $\sigma_{\text{osc}}(\sigma_*)$ in (2.10) and (2.11).

In particular, we find that for $n = 2, 4$ in the potential (1.1) the signs of the non-linearity parameters f_{NL} and g_{NL} oscillate as a function of σ_* . Therefore, even if $r_{\text{dec}} \ll 1$, it is always possible to find regions where the non-Gaussianities are accidentally suppressed and do not conflict current observational bounds. For example, from (2.10) we see that $f_{\text{NL}} \sim 0$ for $r_{\text{dec}} \ll 1$ whenever $\sigma_{\text{osc}}\sigma_{\text{osc}}''/(\sigma_{\text{osc}}')^2 \sim -1$. Using the definitions (2.3) and (2.4) we find,

$$f'_{\text{NL}}(\sigma_*) = \frac{9}{5}N' \left(g_{\text{NL}} - \frac{4}{3}f_{\text{NL}}^2 \right), \quad (2.12)$$

which gives an estimate $|\Delta\sigma| \sim (g_{\text{NL}}N')^{-1}$ for the typical size of the regions $f_{\text{NL}} \sim 0$. This is larger than the range of field values probed by the curvaton fluctuations produced during inflation, $|\delta\sigma_*| \sim 10^{-5}/N'$, if $g_{\text{NL}} \lesssim 10^5$. Therefore, for $g_{\text{NL}} \lesssim 10^5$ we may conclude that the regions $f_{\text{NL}} \sim 0$ correspond to a self-consistent choice of initial conditions and are not destabilized by the fluctuations produced during inflation.

3. Renormalizable potential

The special case of a quartic interaction term in the potential,

$$V = \frac{1}{2}m^2\sigma^2 + \lambda\sigma^4, \quad (3.1)$$

can be discussed using the analytical estimates presented in [10]. If the interaction dominates over the quadratic term at the time of inflation, the curvaton oscillations start in an effectively quartic potential. As the amplitude of the oscillating field decreases, the quartic term dilutes away and the potential becomes quadratic. Assuming the universe remains radiation dominated until the curvaton decay, $r_{\text{dec}} \ll 1$,

the envelope of the oscillating curvaton in the quadratic regime is given by

$$\sigma_{\text{as}}(t) \simeq \frac{\sigma_{\text{osc}}(\sigma_*)}{(mt)^{\frac{3}{4}}}. \quad (3.2)$$

The function $\sigma_{\text{osc}}(\sigma_*)$ can be estimated using Eq. (4.9) in [10], which assumes $\lambda\sigma_*^2 \gtrsim m^2$ and is derived to leading order precision in $r_{\text{dec}} \ll 1$. In approaching the quadratic limit, $\lambda\sigma_*^2 \ll m^2$, the analytical estimates of [10] can no longer be used to obtain quantitative results but the qualitative features remain correct.

To leading order in r_{dec} , Eqs. (2.10) and (2.11) read

$$f_{\text{NL}} \simeq \frac{5}{3r_{\text{dec}}} \left(1 + \frac{\sigma_{\text{osc}}\sigma''_{\text{osc}}}{(\sigma'_{\text{osc}})^2} \right) \quad (3.3)$$

$$g_{\text{NL}} \simeq \frac{50}{27r_{\text{dec}}^2} \left(\frac{\sigma_{\text{osc}}^2\sigma'''_{\text{osc}}}{(\sigma'_{\text{osc}})^3} + \frac{3\sigma_{\text{osc}}\sigma''_{\text{osc}}}{(\sigma'_{\text{osc}})^2} \right), \quad (3.4)$$

and by substituting (3.2) into these, we find (semi)analytical predictions for f_{NL} and g_{NL} . The results are illustrated in Fig. (1).

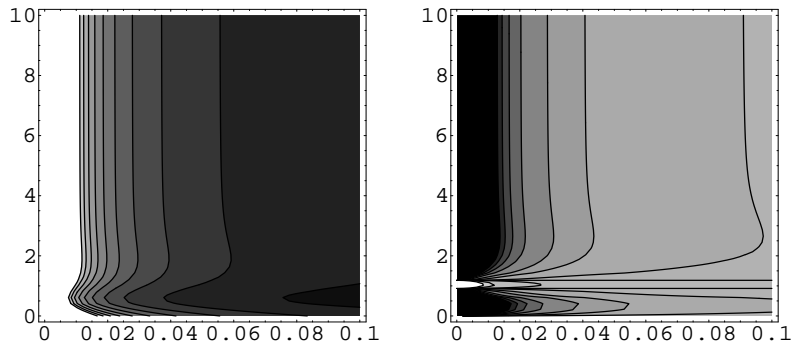


Figure 1: Contour plots of f_{NL} (left panel) and g_{NL} (right panel) with variables r_{dec} and $\sqrt{\lambda}\sigma_*/m$ as x and y axes, respectively. On the left panel, the contours run from 0 (black) to 100 (white) with spacing of 10. On the right panel, they run with spacing of 500 from -5000 (black) to 0 (white).

Although the $n = 0$ case does not result into oscillatory behaviour of $\zeta(\sigma_*)$, non-monotonous features appear when considering derivatives of $\zeta(\sigma_*)$, i.e. the coefficients N'', N''' etc. in (2.1). These features become the more pronounced the higher the order of the derivative $N^{(m)}$ is. This can also be observed in Fig. (1) where both f_{NL} and g_{NL} display non-monotonous behaviour as a function of σ_* in the region $\lambda\sigma_*^2 \sim m^2$. For f_{NL} the non-monotonous features are very mild but g_{NL} shows a significantly more sensitive dependence on σ_* .

As discussed in [10], for $\lambda\sigma_*^2 \sim m^2$ the transition from the quartic to the quadratic part of the potential takes place soon after the onset of oscillations when σ and $\dot{\sigma}$ still act as independent degrees of freedom. These quantities in general do not have

a similar dependence on the initial field value σ_* . Variations of σ_* therefore affect the effective equation of state of the oscillating curvaton in a non-trivial fashion and this is the origin of the structure seen in Fig. (1). If $\lambda\sigma_*^2 \gg m^2$ or $\lambda\sigma_*^2 \ll m^2$, no similar structure is seen. In the former case, the transition into quadratic region happens when the dynamics of the oscillating curvaton is already well described by a single dynamical degree of freedom, the amplitude σ . In the latter case the potential is almost Gaussian from the beginning.

4. Non-renormalizable potentials

The discussion in the preceding section, together with the oscillatory behaviour of ζ presented in [10], leads to an expectation that for non-renormalizable curvaton potentials the naïve estimates $f_{\text{NL}} \sim 1/r_{\text{dec}}$ and $g_{\text{NL}} \sim f_{\text{NL}}^2$ can be violated for a range in the parameter space. It is however not obvious at all how large this range might be. Since the analytical approximations used in the previous section cannot be applied to non-renormalizable potentials, we use numerical methods to track the dynamics at hand.

To calculate the values of f_{NL} and g_{NL} for the non-quartic cases, we use code developed for [10] to compute the values numerically using Eqs. 2.3 and 2.4. To obtain the derivatives, we calculate N for five different initial conditions separated by a spacing a , and then use five-point stencil to calculate the first, the second and the third derivative of N . We adjust the stepping a so that numerical noise is minimized. Furthermore, we adjust a for each pixel independently.

4.1 Qualitative features and differences from naïve expectations

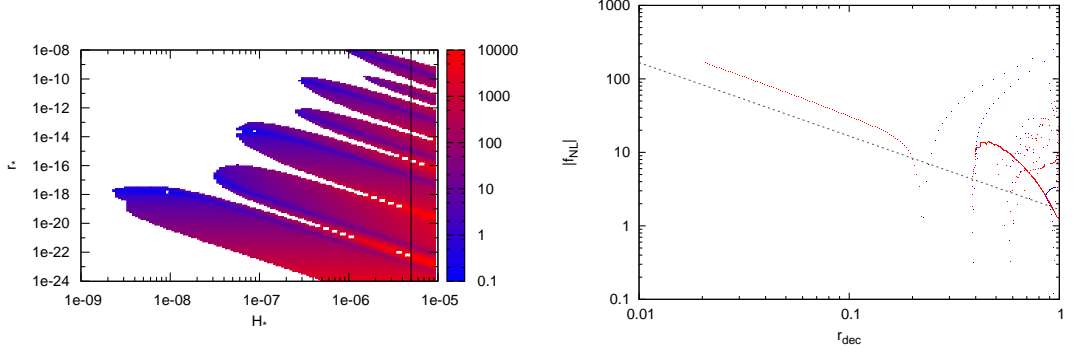
For all choices of m and n , the parameter space is divided into two areas by a line where the quadratic and the non-quadratic terms are equal for the initial curvaton field value, i.e.,

$$\frac{1}{2}m^2\sigma_*^2 = \lambda\frac{\sigma_*^{n+4}}{M^n}.$$

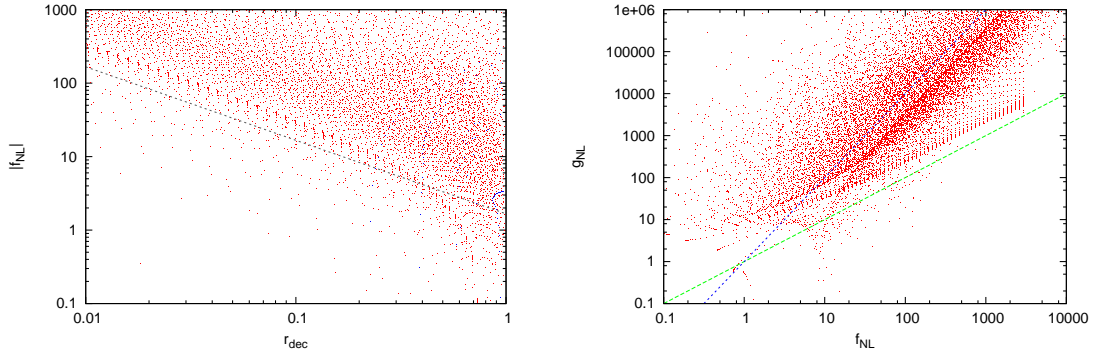
Below this quadratic line we should recover the behaviour predicted analytically for the quadratic case. Above this line the self-interactions modify the behaviour substantially.

For $n = 6$ case the behaviour in the non-quadratic regime is smooth and qualitatively in close resemblance with the case $n = 0$, which was described in the previous section. This is due to the fact that if $n \geq 6$, the field does not oscillate in the non-renormalizable part of the potential at all. However, for the cases $n = 2$ and $n = 4$ large oscillations of ζ as a function of its parameters and initial conditions are present in the non-quadratic regime as described in [10]. Here the expressions $f_{\text{NL}} \sim 1/r_{\text{dec}}$ and $f_{\text{NL}}^2 \sim g_{\text{NL}}$ provide only very rough estimates of the non-linearity parameters, and in the interaction dominated region the actual values of f_{NL} and g_{NL}

can deviate significantly from these estimates. This behaviour can be traced back to the terms including derivatives of σ_{osc} in the Eqs. (2.10) and (2.11).



(a) $|f_{\text{NL}}|$ plotted against the initial conditions r_* and H_* . (b) $|f_{\text{NL}}|$ plotted against r_{dec} for a fixed value $H_* = 5 \times 10^{-6}$, corresponding to the vertical stripe in Fig. 2(a). Red points correspond to $f_{\text{NL}} > 0$ and blue points to $f_{\text{NL}} < 0$.



(c) $|f_{\text{NL}}|$ plotted against r_{dec} for all values of H_* in Fig. 2(a). Red points correspond to $f_{\text{NL}} > 0$ and blue points to $f_{\text{NL}} < 0$. (d) $|g_{\text{NL}}|$ plotted against $|f_{\text{NL}}|$ for all the points in 2(a). The green line corresponds to the linear relation $|g_{\text{NL}}| \sim |f_{\text{NL}}|$ and the blue line to the quadratic relation $|g_{\text{NL}}| \sim |f_{\text{NL}}|^2$.

Figure 2: The behaviour of $|f_{\text{NL}}|$ and $|g_{\text{NL}}|$ for $n = 4$ and $m = 10^{-12}$.

In Fig. 2(a) we have plotted the value of $|f_{\text{NL}}|$ against the initial conditions r_* and H_* . The vertical line in this figure corresponds to a range of parameters, corresponding to the fixed value of $H_* = 5 \times 10^{-6}$, for which $|f_{\text{NL}}|$ is plotted against r_{dec} in Fig. 2(b). Here f_{NL} can be seen oscillating around the $1/r_{\text{dec}}$ -estimate. Oscillations arise from the derivative terms present in Eq. (2.10), which describe the impact of the self-interaction terms on the dynamics of the curvaton. Most points give rise to a larger f_{NL} than one would expect from the estimate $1/r_{\text{dec}}$, however since f_{NL} actually changes sign, points can always be found where f_{NL} is arbitrarily close to zero. In Fig. 2(b) several different values of $|f_{\text{NL}}|$ correspond to a given point r_{dec} since different choices of initial conditions can be degenerate yielding the same r_{dec} .

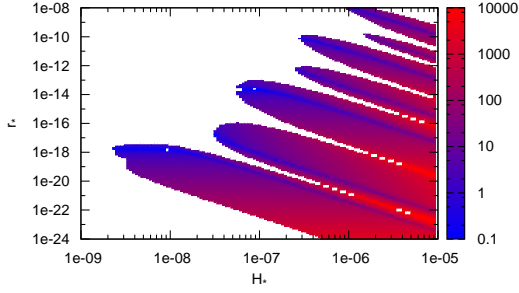
In Fig. 2(c) we plot again $|f_{\text{NL}}|$ against r_{dec} , but we no longer constrain H_* , but instead plot this for all points in Fig. 2(a). Again each point corresponds to a set of parameters producing the observed final amplitude of the primordial perturbations. As we allow H_* to take different values, a family of curves is drawn, where each curve is similar to the curve present in 2(b), resulting into the noisy scatter present in the Fig. 2(c). It is also noteworthy that for given fixed value of r_{dec} , there are multiple sets of parameters which all give the same final amplitude for the perturbations, but different value of f_{NL} (and g_{NL}).

In Fig. 2(d) the value of $|g_{\text{NL}}|$ is plotted against $|f_{\text{NL}}|$. Here three contributions can be clearly distinguished: The $1/r_{\text{dec}}$ -relation arising while in the quadratic regime, the $1/r_{\text{dec}}^2$ -relation in the non-quadratic regime that is due to self-interactions, and scatter around those lines due to the oscillations caused by the self-interactions. This scatter can be understood by considering Fig. 2(b) where f_{NL} can be seen oscillating around the analytical estimate. Plotting g_{NL} against r_{dec} would produce a qualitatively similar plot as Fig. 2(b) showing the oscillations around the $1/r_{\text{dec}}$ and $1/r_{\text{dec}}^2$ estimates deriving from the terms in eq. (2.10). However, in general f_{NL} and g_{NL} do not oscillate with the same phase, and hence when plotting g_{NL} against f_{NL} , scatter is created.

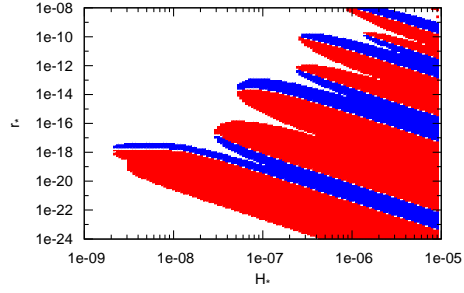
In Fig. 3(a) - 3(d) the magnitudes and signs of f_{NL} and g_{NL} are plotted when scanned through different initial conditions. Here again the oscillatory features can be clearly distinguished as both f_{NL} and g_{NL} oscillate in the regime initially dominated by the non-quadratic interaction. Moreover it is worth emphasizing that not only does the absolute magnitude of f_{NL} and g_{NL} show oscillatory behaviour in this regime, but also their signs change along the oscillations as shown in Fig. 3(b) and 3(d). Furthermore the oscillations of f_{NL} and g_{NL} have different periods and phases, i.e. the zeros of f_{NL} and g_{NL} are not related in a simple fashion.

In Eq. (2.12) we presented a relation between the derivative of f_{NL} with respect to σ_* and the values of g_{NL} and f_{NL} . If $f_{\text{NL}} = 0$, this takes a particularly simple form, $f'_{\text{NL}} = 9/5N'g_{\text{NL}}$, which can be clearly seen in Fig. 3(c).

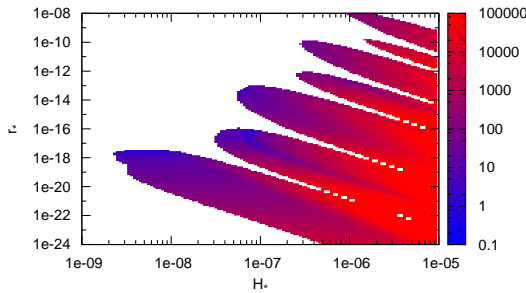
Note that there are two different sources of non-Gaussianity: one is the subdominance of the curvaton at the time of decay r_{dec} , while the other is just the non-linear evolution of curvaton perturbations, encoded in the function σ_{osc} in Eqs. (2.10) and (2.11). Even if $r_{\text{dec}} \sim 1$, large non-Gaussianity can be generated by the evolution of the curvaton. For example, from Eq. (2.10) we see that if $\sigma'_{\text{osc}} \rightarrow 0$, f_{NL} can be very large even though $r_{\text{dec}} \sim 1$. This can be understood qualitatively by looking at the expression for the linear part of the curvature perturbation, $\zeta \sim r_{\text{dec}}(\sigma'_{\text{osc}}/\sigma_{\text{osc}})\delta\sigma_*$ [20]. If $\sigma'_{\text{osc}} \rightarrow 0$, we see that we need to increase $\delta\sigma_*$ to keep $\zeta \sim 10^{-5}$. Therefore, the higher order terms become significant in this limit generating large non-Gaussianities, just like in the limit $r_{\text{dec}} \rightarrow 0$.



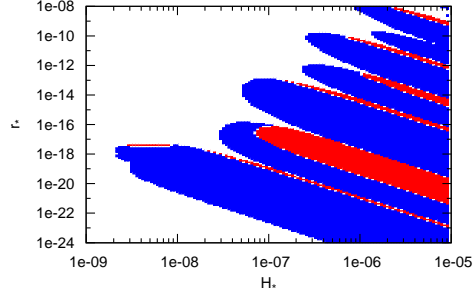
(a) $|f_{\text{NL}}|$ plotted against r_* and H_* .



(b) Sign of f_{NL} plotted against r_* and H_* , where the red color corresponds to positive and blue to negative f_{NL} .



(c) $|g_{\text{NL}}|$ plotted against r_* and H_* .



(d) Sign of g_{NL} plotted against r_* and H_* , where red color corresponds to positive and blue to negative g_{NL} .

Figure 3: Magnitude of $|f_{\text{NL}}|$ and $|g_{\text{NL}}|$ for $n = 4$ and $m = 10^{-12}$.

4.2 Allowed regions of parameter space

In Figs. 5 - 7 we have plotted the points in the parameter space which are compatible with observations of the primordial perturbations. These points give rise to the observed amplitude of the perturbations while producing f_{NL} and g_{NL} which are within the current observable limits.

The range of the initial conditions H_* and r_* has been chosen so that all interesting features should be within the plots. H_* is also bounded from above, $H_* \lesssim 10^{-5}$, to prevent the excessive production of primordial tensor modes and at least an order of magnitude smaller to keep the inflaton perturbations negligible.

Limits for f_{NL} are given by the WMAP 5-year data [18], $-9 < f_{\text{NL}} < 111$. Although in [23] a more stringent constraint for f_{NL} is given as $-4 < f_{\text{NL}} < 80$, we conservatively use the limit provided in [18]. Regarding the limits for g_{NL} , we require that g_{NL} is the range $-3.5 \times 10^5 < g_{\text{NL}} < 8.2 \times 10^5$ as given in [24]. Note that these limits have been derived assuming $f_{\text{NL}} \sim 0$, which here is not the case

in general. However, the bounds for f_{NL} seem to be much more constraining in our case, and relaxing the limits for g_{NL} even by an order of magnitude would not enlarge the allowed area of the parameter space significantly. Thus we adopt this limit for reference purposes¹.

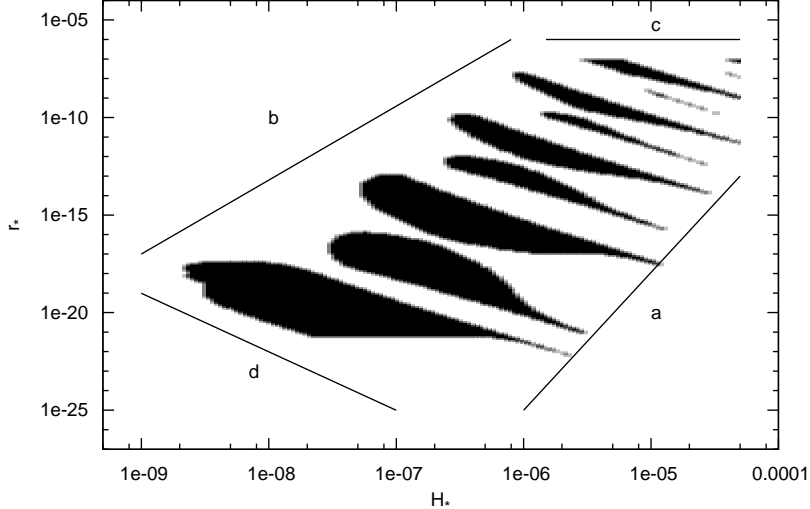


Figure 4: A schematical illustration of the different cuts limiting the allowed area in the parameter space.

In Fig. 4 we give an illustration of the different features limiting the allowed area of the parameter space. The observational limits for f_{NL} and g_{NL} constrain the allowed area in the very subdominant regions of the parameter space, as depicted in Fig. 4 by the line *a*. Other constraints shown in Fig. 4 arise from the internal consistency of the specific curvaton scenario studied in the present paper. The bound *b* is obtained because otherwise the initial perturbations would be too small to produce the observed amplitude. The bound *c* reflects the requirement that the curvaton should be massless, or $V'' < H_*^2$, which is necessary for the generation of curvaton perturbations during inflation. Because of the subdominance of the curvaton, the realistic bound should arguably be a few orders of magnitude tighter. However, a change of an order of magnitude moves the actual cut by a very small amount in the log-log plots.

Finally, the bound *d* guarantees the absence of the isocurvature modes in dark matter perturbations and corresponds to the limit on the curvaton decay width given

¹Recently, the authors of [25] have obtained limits on g_{NL} without assuming $f_{\text{NL}} = 0$ by using N-point probability distribution function. However, their constraint on g_{NL} is similar to that of [24].

in (2.9).

It should be noted, that limits b , c and d in Fig. 4 were already present in [10], so that the non-Gaussianity limit a is the only new limiting ingredient provided by the current work on the space of parameters.

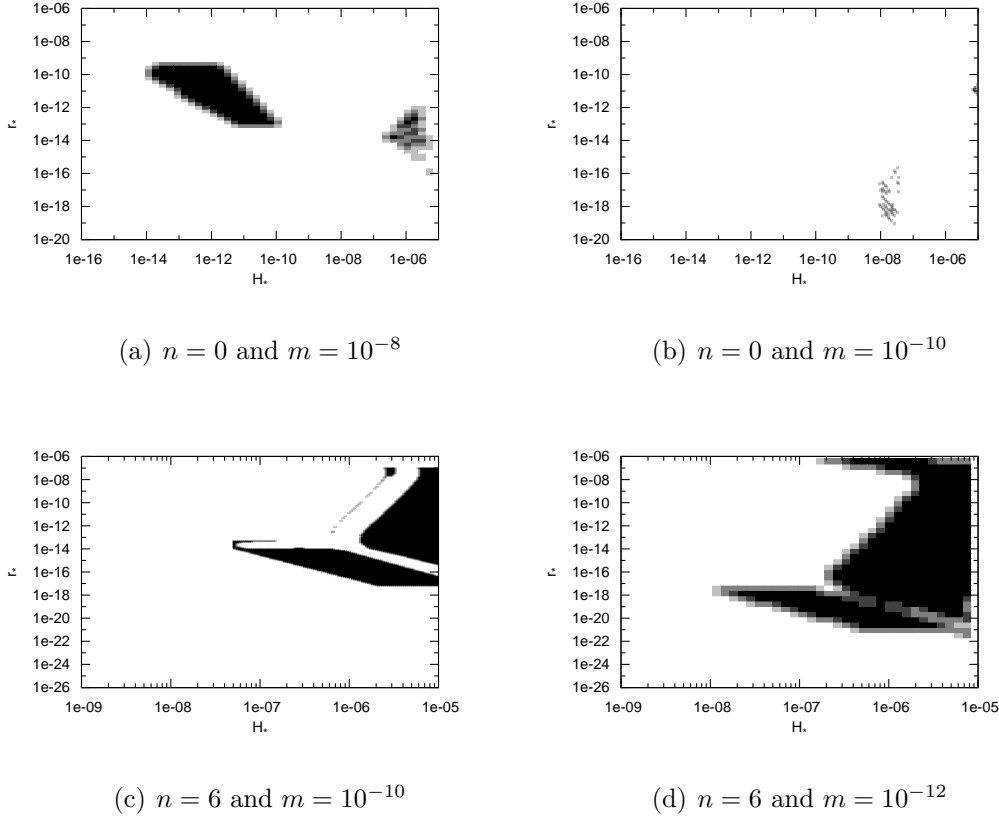


Figure 5: Dark areas correspond to the allowed areas in the parameter space with $-9 < f_{\text{NL}} < 111$ and $-3.5 \times 10^5 < g_{\text{NL}} < 8.2 \times 10^5$ for $n = 0$ and $n = 6$.

As explained in the previous sections, in the regions where the quadratic part of the potential dominates already initially, the dynamics are essentially linear, and the simple results apply. As a consequence, σ_{osc} dependence in Eqs. (2.10) and (2.11) disappears. Therefore these regions are characterized by the smooth continuous allowed area as shown in Figs. 5 - 7, which can be found in the lower left are in the plots. The total area of the allowed region depends on the values of m and n ; e.g. for $n = 4$ and $m = 10^{-8}$ this quadratic area is much larger than for, say, $n = 4$ and $m = 10^{-14}$.

As mentioned previously, $n = 0$ and $n = 6$ do not display extended oscillatory regions. Hence the plots in Fig. 5 remain smooth also in the regime where the self-interaction dominates.

The cases $n = 2$ and $n = 4$ are however characterized by significant oscillatory

features, as discussed in the previous sections. Due to these oscillations, the allowed region consists of isolated patches in the interaction dominated regime. As can be seen in the figures, the size of these patches decreases as we decrease the (bare) mass m , since this tends to make the curvaton more subdominant at the time of decay, decreasing the viable area.

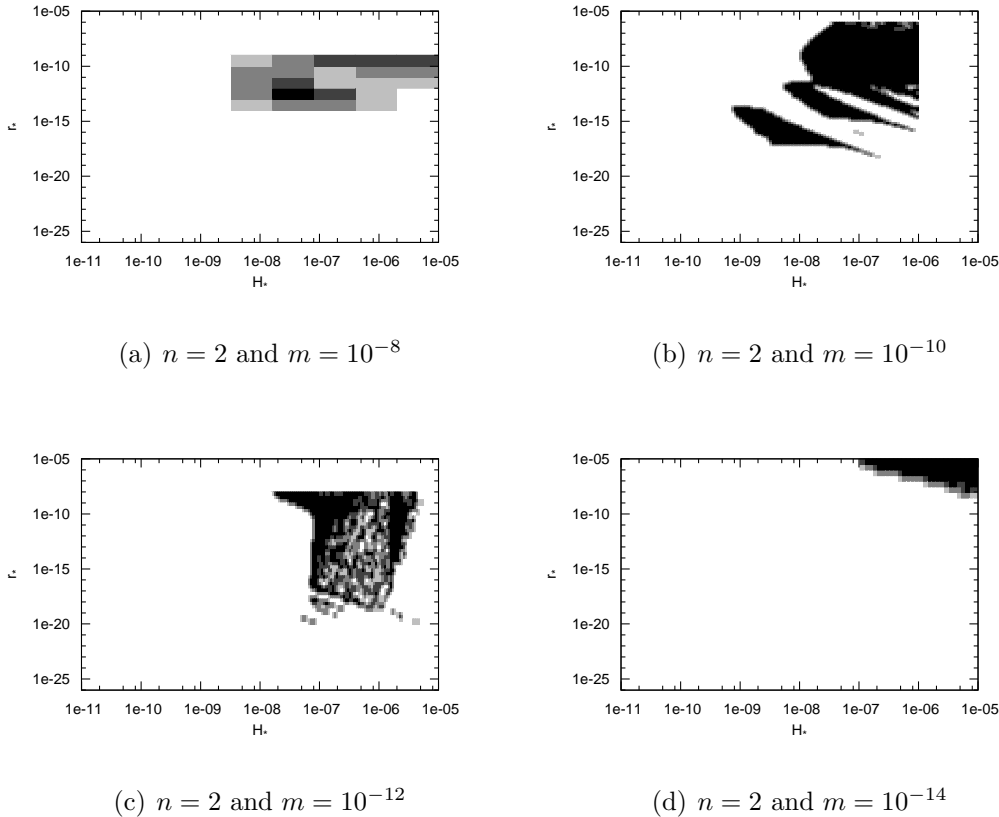


Figure 6: Dark areas correspond to the allowed areas in the parameter space where $-9 < f_{\text{NL}} < 111$ and $-3.5 \times 10^5 < g_{\text{NL}} < 8.2 \times 10^5$ for $n = 2$.

5. Discussion

It seems plausible that the curvaton, like any other scalar field, has some self-interactions. These self-interactions can have a profound effect on the dynamical evolution of the curvaton field and its perturbations, as was discussed in [10] (and in [4, 5]), where we studied the amplitude of the curvature perturbation in self-interacting curvaton models defined by Eq. (1.1). In the present paper we have focussed on the non-Gaussianities of the curvature perturbations by computing the non-linearity parameters f_{NL} and g_{NL} for all the model parameters for which $\zeta \sim 10^{-5}$.

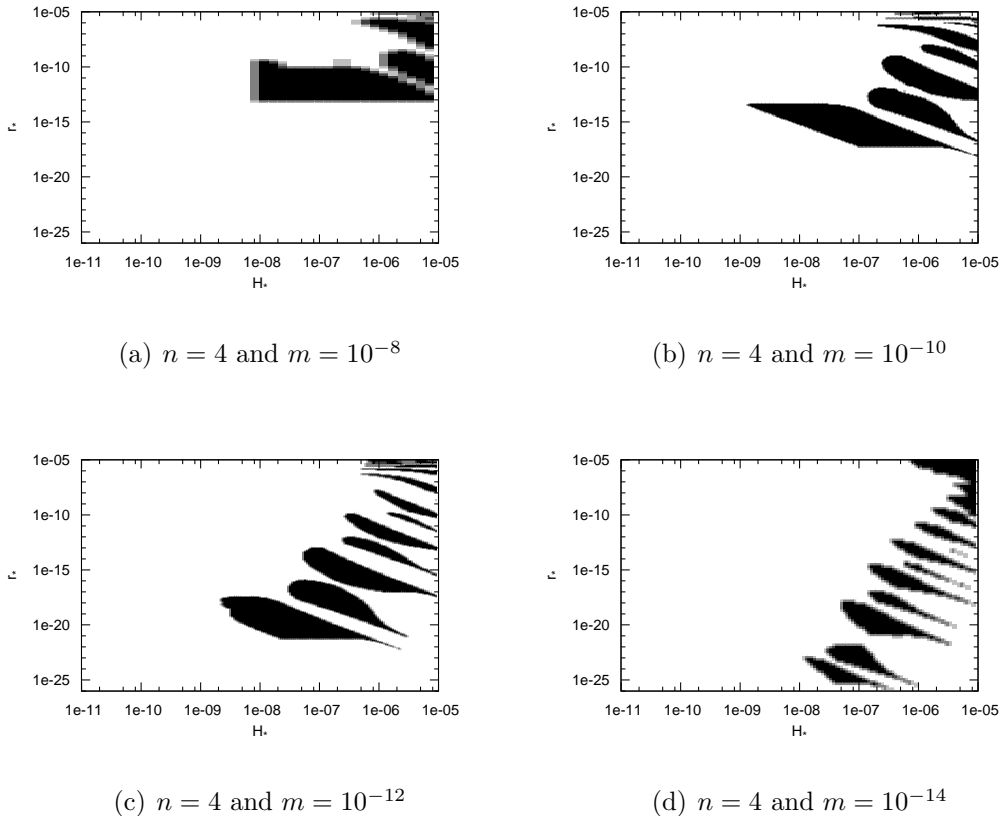


Figure 7: Dark areas correspond to the allowed areas in the parameter space where $-9 < f_{\text{NL}} < 111$ and $-3.5 \times 10^5 < g_{\text{NL}} < 8.2 \times 10^5$ for $n = 4$.

When the curvaton has some self-interactions, the non-Gaussian statistics of the curvature perturbation can be quite different from that produced in the simplest model with a quadratic potential. In the quadratic curvaton model, the magnitude of f_{NL} in the limit $r_{\text{dec}} \ll 1$ is determined by the curvaton energy density at the time of its decay, $f_{\text{NL}} \sim 1/r_{\text{dec}}$. However, the prediction of f_{NL} can significantly deviate from this simple estimate if the curvaton has non-renormalizable self-interactions. As seen from Fig. 2(c), for such models the values of f_{NL} scatter around the estimate $1/r_{\text{dec}}$ and typically end up being slightly larger than in the quadratic case. Thus a very subdominant curvaton is not favoured because it tends to yield a value of f_{NL} which is in excess of the observational bounds $|f_{\text{NL}}| \lesssim 100$ [18, 23].

However, it is interesting to note that even if $r_{\text{dec}} \ll 1$, there exists regions in the parameter space with $|f_{\text{NL}}| < \mathcal{O}(1)$. This is because the value of f_{NL} oscillates and changes its sign, as is illustrated in Fig. 2(a) for $n = 4$. However, even if $f_{\text{NL}} < \mathcal{O}(1)$, the non-linearity parameter for the trispectrum g_{NL} can be very large, as can be seen in Fig. 2(d). In these regions the self-interacting curvaton scenario gives rise to a rather non-trivial non-Gaussian statistics characterized by a large trispectrum and a

vanishing bispectrum. Such a situation, discussed already in [5], appears to be rather generic in self-interacting curvaton models, and possible for a wide, albeit restricted, range of model parameters.

Another interesting feature of the curvaton model with self-interactions is that large non-Gaussianities $|f_{\text{NL}}| \gg \mathcal{O}(1)$ can be generated even if the curvaton dominates the energy density at the time of its decay, $r_{\text{dec}} \sim 1$. Recently in [26] it was shown that for $r_{\text{dec}} \sim 1$, the entropy production at the curvaton decay can leave an imprint on the spectrum of primordial gravitational waves, which in principle could be observable. If the curvaton had no self-interactions, such a signal would imply that no large non-Gaussianity could be generated by the curvaton fluctuations. This is clearly not the case when the self-interactions are included, which serves to demonstrate that the self-interactions can significantly affect the generic features of the curvaton scenario.

Another interesting feature that is clearly visible in Fig. 2(d) is the breakdown of the relation of $g_{\text{NL}} = -(10/3)f_{\text{NL}}$ which holds true for the quadratic potential. For the self-interacting curvaton a large number of points, each corresponding to an allowed set of parameter values, can be seen to fall into the region with $|g_{\text{NL}}| > |f_{\text{NL}}|$. If the interactions are small compared to the quadratic part, the linear relation $g_{\text{NL}} = -(10/3)f_{\text{NL}}$ gets replaced by $g_{\text{NL}} \sim -f_{\text{NL}}^2$ [5]. However, when the self-interaction term dominates, both of the above relations can be violated, as is seen from Fig. 2(d). There is nevertheless a tendency for the points to be concentrated around the lines $|g_{\text{NL}}| \sim |f_{\text{NL}}|$ and $|g_{\text{NL}}| \sim |f_{\text{NL}}^2|$.

We should also like to point out that in the quadratic case with $|f_{\text{NL}}| \gg 1$, the signs of f_{NL} and g_{NL} are respectively positive and negative. In contrast, in the cases studied here, the signs can well be the same. This feature provides an obvious departure from the quadratic case and could offer an experimental possibility to constrain the curvaton self-interaction.

It is evident from the figures presented in Sect. 4 that the self-interacting curvaton model provides us a rich tapestry of features, constrained in a highly non-trivial way by the observational limits on non-Gaussianity. As we have argued here, in the presence of self-interactions the relative signs of f_{NL} and g_{NL} and the functional relation between them is typically modified from the quadratic case. Thus the non-linearity parameters taken together, in possible conjunction of other cosmological observables such as tensor perturbations, may offer the best prospects for constraining the physical properties of the curvaton.

Acknowledgments

This work is supported in part by the Grant-in-Aid for Scientific Research from the Ministry of Education, Science, Sports, and Culture of Japan No. 19740145 (T.T.), by the EU 6th Framework Marie Curie Research and Training network "UniverseNet"

(MRTN-CT-2006-035863), by the Academy of Finland grants 114419 (K.E.) and 130265 (S.N.) and by the Magnus Ehrnrooth Foundation (O.T.).

References

- [1] K. Enqvist and M. S. Sloth, Nucl. Phys. B **626**, 395 (2002) [arXiv:hep-ph/0109214]; D. H. Lyth and D. Wands, Phys. Lett. B **524**, 5 (2002) [arXiv:hep-ph/0110002]; T. Moroi and T. Takahashi, Phys. Lett. B **522**, 215 (2001) [Erratum-ibid. B **539**, 303 (2002)] [arXiv:hep-ph/0110096]; A. D. Linde and V. F. Mukhanov, Phys. Rev. D **56** (1997) 535 [arXiv:astro-ph/9610219]; S. Mollerach, Phys. Rev. D **42** (1990) 313.
- [2] D. Langlois and F. Vernizzi, Phys. Rev. D **70** (2004) 063522 [arXiv:astro-ph/0403258]; G. Lazarides, R. R. de Austri and R. Trotta, Phys. Rev. D **70** (2004) 123527 [arXiv:hep-ph/0409335]; F. Ferrer, S. Rasanen and J. Valiviita, JCAP **0410** (2004) 010 [arXiv:astro-ph/0407300]; T. Moroi, T. Takahashi and Y. Toyoda, Phys. Rev. D **72**, 023502 (2005) [arXiv:hep-ph/0501007]; T. Moroi and T. Takahashi, Phys. Rev. D **72**, 023505 (2005) [arXiv:astro-ph/0505339]; K. Ichikawa, T. Suyama, T. Takahashi and M. Yamaguchi, Phys. Rev. D **78**, 023513 (2008) [arXiv:0802.4138 [astro-ph]]; D. Langlois, F. Vernizzi and D. Wands, JCAP **0812** (2008) 004 [arXiv:0809.4646 [astro-ph]].
- [3] K. Dimopoulos, G. Lazarides, D. Lyth and R. Ruiz de Austri, Phys. Rev. D **68** (2003) 123515 [arXiv:hep-ph/0308015].
- [4] K. Enqvist and S. Nurmi, JCAP **0510**, 013 (2005) [arXiv:astro-ph/0508573].
- [5] K. Enqvist and T. Takahashi, JCAP **0809**, 012 (2008) [arXiv:0807.3069 [astro-ph]].
- [6] K. Enqvist, S. Nurmi and G. I. Rigopoulos, JCAP **0810** (2008) 013 [arXiv:0807.0382 [astro-ph]].
- [7] Q. G. Huang, JCAP **0811**, 005 (2008) [arXiv:0808.1793 [hep-th]].
- [8] M. Kawasaki, K. Nakayama and F. Takahashi, JCAP **0901**, 026 (2009) [arXiv:0810.1585 [hep-ph]].
- [9] P. Chingangbam and Q. G. Huang, JCAP **0904**, 031 (2009) [arXiv:0902.2619 [astro-ph.CO]].
- [10] K. Enqvist, S. Nurmi, G. Rigopoulos, O. Taanila and T. Takahashi, JCAP **0911**, 003 (2009) [arXiv:0906.3126 [astro-ph.CO]].
- [11] A. Chambers, S. Nurmi and A. Rajantie, arXiv:0909.4535 [astro-ph.CO].
- [12] K. Enqvist and T. Takahashi, JCAP **0912**, 001 (2009) [arXiv:0909.5362 [astro-ph.CO]].
- [13] D. H. Lyth, C. Ungarelli and D. Wands, Phys. Rev. D **67**, 023503 (2003) [arXiv:astro-ph/0208055].

- [14] A. A. Starobinsky, JETP Lett. **42** (1985) 152 [Pisma Zh. Eksp. Teor. Fiz. **42** (1985) 124]; M. Sasaki and E. D. Stewart, Prog. Theor. Phys. **95**, 71 (1996); M. Sasaki and T. Tanaka, Prog. Theor. Phys. **99**, 763 (1998).
- [15] D. Wands, K. A. Malik, D. H. Lyth and A. R. Liddle, Phys. Rev. D **62** (2000) 043527 [arXiv:astro-ph/0003278]; D. H. Lyth and D. Wands, Phys. Rev. D **68**, 103515 (2003) [arXiv:astro-ph/0306498]; D. H. Lyth, K. A. Malik and M. Sasaki, JCAP **0505**, 004 (2005);
- [16] C. T. Byrnes, S. Nurmi, G. Tasinato and D. Wands, arXiv:0911.2780 [astro-ph.CO].
- [17] D. Wands, N. Bartolo, S. Matarrese and A. Riotto, Phys. Rev. D **66** (2002) 043520 [arXiv:astro-ph/0205253].
- [18] E. Komatsu *et al.* [WMAP Collaboration], Astrophys. J. Suppl. **180**, 330 (2009) [arXiv:0803.0547 [astro-ph]].
- [19] K. A. Malik, D. Wands and C. Ungarelli, fluids,” Phys. Rev. D **67** (2003) 063516 [arXiv:astro-ph/0211602].
- [20] D. H. Lyth and Y. Rodriguez, Phys. Rev. Lett. **95** (2005) 121302 [arXiv:astro-ph/0504045].
- [21] M. Sasaki, J. Valiviita and D. Wands, Phys. Rev. D **74**, 103003 (2006) [arXiv:astro-ph/0607627].
- [22] M. S. Turner, Phys. Rev. D **28** (1983) 1243.
- [23] K. M. Smith, L. Senatore and M. Zaldarriaga, JCAP **0909**, 006 (2009) [arXiv:0901.2572 [astro-ph]].
- [24] V. Desjacques and U. Seljak, arXiv:0907.2257 [astro-ph.CO].
- [25] P. Vielva and J. L. Sanz, arXiv:0910.3196 [astro-ph.CO].
- [26] K. Nakayama and J. Yokoyama, arXiv:0910.0715 [astro-ph.CO].